A Narrowband Imaging Survey for
High Redshift Galaxies
in the Near Infrared[1]

D. Thompson

Max-Planck-Institut für Astronomie, Heidelberg, Germany

Electronic mail: djt@mpia-hd.mpg.de

F. Mannucci

C.A.I.S.M.I.–C.N.R., Florence, Italy

Electronic mail: filippo@arcetri.astro.it

and

S. V. W. Beckwith

Max-Planck-Institut für Astronomie, Heidelberg, Germany

Electronic mail: svwb@mpia-hd.mpg.de

ABSTRACT

A narrowband imaging survey of 276 square minutes of arc was carried out at near infrared wavelengths to search for emission line objects at high redshifts. Most of the fields contained a known quasar or radio galaxy at a redshift that placed one of the strong, restframe optical emission lines (Hα, [O III], Hβ, or [O II]) in the bandpass of the narrowband filter. The area weighted line flux limit over the entire survey was $3.4 \times 10^{-16}\,\mathrm{erg\,cm^{-2}\,s^{-1}}$ (3σ), while the most sensitive limits reached $1.4 \times 10^{-16}\,\mathrm{erg\,cm^{-2}\,s^{-1}}$. Integrating the volume covered by all four optical emission lines in each image yields a total comoving volume surveyed of $1.4 \times 10^5\,\mathrm{Mpc^3}$. Considering only H$\alpha$ emission in the K band ($2.05 < z < 2.65$), where the survey is most sensitive, the survey covered a comoving volume of $3.0 \times 10^4\,\mathrm{Mpc^3}$ to a volume-weighted average star formation rate of $112\,\mathrm{M_\odot\,yr^{-1}}$ (for $H_0 = 50\,\mathrm{km\,s^{-1}\,Mpc^{-1}}$, $\Omega_0 = 1$). This is the most extensive near-infrared survey which is deep enough to have a reasonable chance at detecting strong line emission from an actively star-forming population of galaxies, when measured against simple models of galaxy formation. One emission line candidate was identified in this survey, and subsequently confirmed spectroscopically.

Subject headings: cosmology: observations — early universe — galaxies: formation — infrared: galaxies

---

1. Introduction

The great majority of galaxies began forming their stars early in the history of the universe at observable redshifts greater than 1. Of these, the stars in the spheroidal galaxies – ellipticals, lenticulars, and the bulges of spirals – are thought to be the oldest. It is not known exactly how old the oldest stars are, although the upper age estimates (Coles & Ellis 1994) are in conflict with the age of the universe in some cosmologies (Freedman et al. 1994; Mould et al. 1995). It is also difficult to reconcile very old galaxies with models of structure formation, particularly the cold dark matter models (e.g. Börner, Mo, & Jing 1995; Efstathiou 1995). Identification of the first generations of stars and measurements of their ages are, therefore, of considerable interest to cosmologists.

There is some evidence that galaxy-sized structures existed early. Globular clusters have apparent ages of 14–16 Gyr. Galaxies at redshifts of order 1.5 have been discovered which appear to have evolved stars, thus implying a high redshift of formation (Cowie, Hu, & Songaila 1995, Dunlop, et al. 1996). Quasars are seen to redshifts of order 5 (Schneider, Schmidt, & Gunn 1991) and their hosts represent at least a fraction of the galaxy population. Damped Lyα-absorption line systems, possibly indicative of galaxy disk formation, are also seen to redshifts above 4 (McMahon et al. 1994; Lu et al. 1996). Many high redshift radio galaxies have been identified, and it has been suggested that they represent a stage in the formation of more normal galaxies (Meier 1976, Terlevich 1992, Haenelt & Ress 1993).

There are some very exciting new results suggesting that we are beginning to identify large populations of high-redshift objects. Redshift surveys of complete samples of faint galaxies have turned up a number of interesting sources with $z > 1$ (Ellis, et al. 1996, Cowie, Songaila, & Hu 1996). As many as six potential clusters of galaxies at $z > 2$ have been recently been reported (Francis, et al. 1996; Malkan, Teplitz, & McLean 1996; Efstathiou, 1996). A population of galaxies at $z > 3$ have been identified by Steidel et al. (1996, see also Giavalisco et al. 1996), using a continuum selection technique. And the redshift of the most distant "normal" galaxy known has been climbing rapidly, standing now at $z = 4.55$ with the spectroscopic confirmation of three galaxies associated with a quasar (Hu & McMahon 1996).

The problem with observing the first epochs of star formation is that the signatures of these epochs are not known and are very poorly constrained. It is usually assumed that the first galaxies emitted copiously in the Lyα line of hydrogen (Partridge & Peebles 1967; Tinsley 1977, 1978; Baron & White 1987), though very few examples of Lyα-bright galaxies have been found (Pritchet 1994) despite considerable effort (De Propris et al. 1993; Pritchet & Hartwick 1987, 1990; Thompson, Djorgovski & Trauger 1995 (TDT95); Thompson & Djorgovski 1995; and others). Almost all the surveys for Lyα have been at optical wavelengths and are limited to redshifts below about 6. Recent continuum-based surveys (Steidel & Hamilton 1992, see also Steidel & Hamilton 1993; Steidel, Pettini, & Hamilton 1995) have been very successful in finding young galaxies near redshifts around 3 by looking for Lyman-break objects using broad band

filters. While these galaxies appear to have fairly significant star formation rates $(4\text{–}25 \, \mathrm{M}_\odot \, \mathrm{yr}^{-1}$, see Steidel et al. 1996), they generally have weak or absent Lyα emission despite apparently low dust content.

This paper presents the results of a complementary approach to search for young galaxies, searching for redshifted emission lines of hydrogen and oxygen at wavelengths between 1 and $2.5 \, \mu$m. The main advantage of this approach is that the lines are emitted at much longer rest-frame wavelengths than Lyα and, therefore, suffer considerably less from extinction by dust. Even small amounts of dust, of order 1 visual magnitude, are enough to quench Lyα emission through resonant scattering off neutral hydrogen and even depress the ultraviolet continuum without substantially diminishing the intensity of longer wavelength lines (e.g. Djorgovski & Weir 1990; Charlot & Fall 1993; Mannucci & Beckwith 1995, hereafter MB95). Most of the sources discovered by Steidel and his colleagues do have weak Lyα, indicative of extinction or absorption intrinsic to the source. An additional advantage of the infrared observations is that they can detect the Lyα line at redshifts exceeding 7. A bright population of galaxies at these very high redshifts can only be studied in the infrared and are perhaps already indicated by the presence of quasars at redshifts around 5 (Turner 1991).

Our approach consists of taking deep images through narrow and broad band filters and looking for objects which are relatively brighter in the narrow filter, thus indicating a substantial flux in an emission line. We chose the fields to contain objects with known redshifts which put optical emission lines (Hα, [OIII] λ5007Å, Hβ, or [OII] λ3727Å) in the passbands of the narrow filters. If there is any tendency toward clustering, these objects will pinpoint regions of overdensity.

Variations of this approach have been used before by Boughn, Saluson, & Uson (1986); Collins & Joseph (1988); Thompson, Djorgovski, and Beckwith (1994); Parkes, Collins, & Joseph (1994); Malkan, Teplitz, & McLean (1995); Bunker, et al. (1995); and Pahre & Djorgovski (1995, hereafter PD95), see also Mannucci, Beckwith, & McCaughrean (1994). The main advance of the present work is the use of a wide-field infrared camera constructed specifically to undertake such surveys. The present survey searches about two orders of magnitude more volume in the universe for signatures of emission lines in the infrared than previously accomplished. What is presented below represents the largest area surveyed to date at sensitivities approaching the best in the literature. We assume a cosmology of $H_0 = 50$ and $\Omega_0 = 1$ throughout this paper.

2. Observations

The target fields were selected primarily from the quasar lists of Veron and Veron (1993) and Hewitt & Burbidge (1993). Special emphasis was given to objects with either Hα or [OIII] in the K band, which select the redshift ranges $2.1 < z < 2.6$ and $3.0 < z < 3.6$, respectively. The first range corresponds to the peak comoving density of active nuclei, and may indicate an unusually vigorous period of galaxy formation. Objects in this redshift range have the [O III] and Hβ lines

in the H band and [OII] in the J band, facilitating the spectroscopic confirmation of their redshift. The second redshift range targets an earlier epoch for galaxy formation, and has the [OII] line in the H band. Preference was also given to fields at high galactic lattitude and which transit near zenith at Calar Alto or La Silla to minimize both galactic and atmospheric obscuration. Four fields have no known objects at redshifts sampled by the narrow band filters; these are referred to as *blank fields*. A list of the observations is given in Table 1.

Images were taken in pairs through a narrowband filter and a broadband filter near the same wavelength. A total of 30 image pairs were obtained with exposure times of 1-2 hours through the narrowband filter and 15-30 minutes through the broadband filter. Each image consisted of many subimages of 1 minute integration time each. The different subimages were toward positions differing by approximately $15''$ (dithering), allowing many unregistered images to be combined for background subtraction. The background-subtracted subimages were then registered and combined to produce the final image pairs. All data were obtained in background-limited conditions, and the weather was photometric or nearly so throughout the observations.

Most of the data were obtained at the Calar Alto 3.5m telescope, using the MAGIC cameras (Herbst et al. 1993) with wide-field optics. In this configuration, the NICMOS3 256^2 HgCdTe array images a $207''$ square field of view at $0''.81$ per pixel. There is a slight loss in sensitivity due to the undersampling of the point spread function (PSF) at times of good seeing, but this disadvantage is more than offset by the large field of view available. These data were supplemented with images from the ESO/MPI 2.2m telescope on La Silla. The IRAC2A and IRAC2B (Moorwood et al. 1992) cameras were used with lens system D. These cameras also use NICMOS3 arrays. In this configuration, they have a circular field of view of $180''$ (the corners are vignetted) with $0''.7$ pixels.

3. Data Reduction and Calibration

The data were reduced with the IRAF package using the following procedure: 1) a separate sky frame was constructed for each image using temporally adjacent but spatially offset images, 2) each image was then sky-subtracted and flatfielded using a normalized domeflat, and 3) the flatfielded images were stacked into the final, deep images. The sky frames were typically constructed using 6–12 (depending on atmospheric stability) images taken near the time of each individual exposure, scaled to have the same median sky level. The extremes of the distribution in each pixel were clipped and the remaining combined either with averaging or taking a median. As the fields were relatively devoid of bright objects in the first place, the resulting sky frames were quite clean. The reduced frames (typically 180 images for a 90-minute series through the narrowband filters) were registered on objects visible in the individual images and offset using integer pixel shifts. The stacking was done in a similar manner to the construction of the sky frames, clipping pixels at each end of the distribution (ignoring flagged bad pixels), and averaging

the remaining values. The final stacked images were then trimmed to include only the highest sensitivity regions where both the broadband and narrowband stacks overlap.

Positions were determined for all of the objects on the narrowband images using FOCAS (Jarvis & Tyson 1981, Valdes 1989), with the number of connected pixels set to 4-6, depending on the seeing, and the threshold for detection to 3σ. For our data, these settings recover all objects within the frame that are readily apparent without producing excessive numbers of obviously false detections. Instrumental magnitudes were determined for each object in the broadband and narrowband images through circular apertures using the PHOT routine in IRAF. The photometric aperture was set to twice the seeing full-width at half-max (FWHM), which maximizes the signal-to-noise ratio for faint, point-like sources (TDT95, Howell 1989). Small aperture corrections were then applied as determined from brighter point sources in each individual image. This procedure will underestimate the flux from bright, extended sources, although it should have minimal effect on high-redshift galaxies which subtend only a few seconds of arc. Note that faint sources more extended than $\sim 2''$, corresponding to $\sim$15 kpc at $z = 2.5$, have a lower probability of being identified by FOCAS in the first place.

The magnitude scale was established with the Elias standards (Elias et al. 1982) and the UKIRT faint standard star list (Casali 1992), with the flux density zero points taken from Bessel & Brett (1988). For broadband observations in the K$'$ filter, we assumed that the standard stars had the same magnitude in K$'$ as in the standard K filter. Calibration of the narrowband images was complicated by the presence of 12 hydrogen white dwarf stars among the 34 UKIRT standards[2]. Initially, narrowband magnitudes for the standards were interpolated from their broadband magnitudes, using the filters' central wavelengths and widths. This method is inaccurate when used with hydrogen white dwarf stars, because they have strong absorption lines in the hydrogen line filters (e.g., Paβ and Brγ). To provide accurate calibrations, we assumed that the majority of objects in each frame had no excess emission line flux. Testing this method on photometric data with both white dwarf and subdwarf standards shows the method to be reliable, with an accuracy better than 0.1 mag.

4.   Results

Plots of the (broad−narrow) color vs. narrowband magnitude were constructed for each of the 30 image pairs. Objects with relatively strong emission lines stand well away from the locus of the remaining objects. All of the known AGN showed strong emission line signatures when Hα was in the narrowband filter, while the radio galaxy B3 0806+426 showed strong emission in the [O III] λ5007 Å line. There was only a single strong candidate identified in the survey data, discussed below. A summary of the reduced data (seeing, trimmed field size, and flux limits) are

---

[2]It was also found that FS24 (SA 106-1024) is listed as a variable star.

given in Table 2. Total errors on the determination of the emission-line flux limits are estimated to be $\pm 20\%$, based on multiple measurements of the standard stars.

A color-magnitude diagram for the B2 0149+33A field is presented in Figure 1, which illustrates the selection criteria for candidate emission-line objects. The curved line indicates the 3σ emission-line flux limit, taking into account the uncertainties from both the broad and narrowband images. In this field, the line does not go through the zero color line because the central wavelength of the narrowband filter is near the red end of the broadband filter transmission. The curve was derived in a similar manner to that in Bunker et al. (1995). The horizontal dashed line indicates a 50 Å restframe equivalent width limit for emission lines. This limit is lower than the equivalent Bunker et al. (1995) limits mainly due to the narrower filters used in this survey (1% vs. 1.75%). The diagonal, long-dash line is a color limit, where objects falling to the left of this line are well detected in both the broad and narrowband images. Candidate objects must lie above the equivalent width limit and to the left of the 3σ flux limit. We note that an object with an infinite equivalent width emission line would have a color of 3.1 (for this field, off the top of the plot), independent of its magnitude. Many of the objects with this color lay near the edges of the narrowband images in regions where the noise was a little higher than in the center of the image. They were inspected carefully by eye, and dropped from further consideration if they appeared to be spurious detections. Finally, the image pairs were "blinked" on a workstation monitor to determine the quality of the candidates by inspection.

4.1. The B2 0149+33 field

The quasar ($z = 2.431$) shows strong emission with a line flux of 8.4×10^{-15} erg cm^{-2} s^{-1} (labelled "QSO" in Figure 1). The restframe equivalent width of the emission line, as derived from the broad and narrowband images, is 130 Å. There is a companion galaxy $2\rlap{.}''2$ to the southwest at PA= $249°$ which is evident in both the broad and narrowband images. We subtracted a point-spread-function from the quasar image to check for excess flux in the companion galaxy; none was found – the companion is plotted with an open circle on Figure 1. The quasar shows a damped Lyα system at $z = 2.133$ (Wolfe et al. 1986). If this galaxy is the absorber, it lies 18 kpc from the line of sight (H$_0 = 50$, $\Omega_0 = 1$). It has a K$'$ magnitude of 17.85. There are several other fainter galaxies which lie within $15''$ of the quasar.

Object 39 in Figure 1 is the strongest emission-line candidate in this survey with a derived emission line flux of 6.5×10^{-16} erg cm^{-2} s^{-1}, a 10σ emission-line detection in this field. It is an extended object with a K$'$ magnitude of 18.52 lying $50\rlap{.}''1$ from the quasar at PA $295\rlap{.}°1$. The restframe equivalent width for the emission line is 125 Å, which is high, though not unreasonable, for nearby starburst galaxies. If this galaxy is at the same redshift as the quasar, the line flux would correspond to a restframe line luminosity of 2.8×10^{43} erg s^{-1}. Using the empirical conversion

of Hα luminosity to star formation rate of Kennicutt (1983, see also MB95), the star formation rate is $250 \, M_\odot \, yr^{-1}$. Preliminary reduction of spectra of this object, obtained in the K band at UKIRT, confirm the emission line, and will be discussed more extensively in a separate paper (Beckwith et al. 1997). The images of this field are shown in Figure 2.

Object 27 corresponds to a short, thin arc in the narrowband image, whose width is less than the seeing FWHM. Although there is a faint galaxy at this position in the broadband image, this candidate is considered to be a spurious detection.

4.2. Survey limits

Several near-infrared searches for emission-line objects have been published during the last few years (TDB94, PD95, Bunker et al. 1995, Parkes et al. 1994) and a few others have been undertaken (Malkan, Teplitz, & McLean 1995). All make use of narrowband imaging to identify candidate emission line objects. Figure 3 is a comparison of several surveys in the observed quantities of area vs. line flux. The relative advantages of the approach adopted here is evident from this figure. The area covered in the present survey is approximately two orders of magnitude greater than the other most recent works, those of Bunker et al. (1995) and PD95. The flux limits of the present work are about four times higher than that in PD95, but as discussed below the area coverage has significant advantages to search for the emission signatures expected from young galaxies at high redshift.

4.3. Restframe Limits

While Figure 3 compares surveys in observed coordinates, the survey limits can be better expressed in restframe coordinates within an assumed cosmology. Although the full parameter space is 3-dimensional (MB95, TDT95), with axes of comoving volume density, line luminosity, and redshift, it is generally viewed in projection along the redshift axis. Working in the restframe allows a direct comparison between the survey results and models of galaxy and star formation rates versus the comoving volume density of objects. To calculate the total volume sampled by the survey, we include the five strong lines: Hα, Hβ, [OIII]λ5007, [OII]λ3727, and Lyα. Each of these appears in the narrowband filters at different redshifts. Each imaged field thus covers five sampled volumes at different redshifts. The total volume covered by the survey in the four optical lines (Lyα is considered separately, below) is $1.4 \times 10^5 \, Mpc^3$ for $H_0 = 50 \, km \, s^{-1} \, Mpc^{-1}$, $\Omega_0 = 1$.

Assuming a Poisson distribution (no clustering), the probability, $P_0(V)$, that *no* objects are present in the sampled volume, V, is $P_0(V) = \exp(-\rho V)$, where ρ is the average density of objects. Prior surveys similar to this one have calculated their volume density simply as the inverse of the volume surveyed, giving only a 63% chance of detecting anything. For this survey, we adopt a more conservative 90% probability of detecting *at least* one object in the sampled volume, which

requires that $0.9 \leq 1 - \exp(-\rho V)$, implying that $\rho \geq 2.3/V$. Both the observed frame limits plot (Figure 3) and the restframe limits discussed below incorporate this formula to correct the survey to 90% detection probability. All of the data taken from the literature and used here has been corrected for this factor of 2.3 as well.

Line luminosities are converted into equivalent star formation rates by assuming a linear correlation between the two quantities and adopting the normalization for Hα given by Kennicutt (1983) and assuming line ratios relative to Hα as in MB95. The survey limits on the number density of objects with various line fluxes are then transformed into volume density of objects with different star formation rates at discrete redshift intervals. These relationships may be compared directly with models of galaxy formation in the early universe, discussed in the next section.

It is important to emphasize, however, that the survey limits plotted in following the 4 figures assume no obscuration by dust, and therefore represent lower limits to the true star formation rate. Even without considering resonant scattering of the Lyα photons, simple dust absorption, assuming a galactic extinction law and $E_{(B-V)} = 0.3$ (corresponding to $\sim 1^m$ of visual extinction), would imply that the true star formation rates are higher than that of no obscuration by a factor of 2 at Hα, 2.8 at Hβ, 3.6 at [O II], and 16 at Lyα (Seaton 1979). We have included in the following plots an arrow showing the magnitude and direction that an extinction of $E_{(B-V)} = 0.3$ would have on the plotted survey limits.

4.3.1. Galaxy Formation Models

Figures 4–7 compare the survey limits to the expected comoving density and luminosity of forming galaxies, taking into account various star formation histories and mass evolution. The model details are described more thoroughly in MB95 and are only summarized here. These models estimate the *minimum* density of young galaxies as a function of star formation rate which are necessary to produce the local population of elliptical galaxies. The estimated densities depend on the normalization, ϕ^*, of the local galaxy luminosity function. We assume ϕ^* as given in Baron & White (1987), though this has subsequently been revised upwards by a factor of about 2.2 by the most recent redshift surveys, as in Ellis et al. (1996). Use of this higher normalization would increase our model galaxy densities by this factor.

We consider three classes of models, ranging from strong bursts to distributed star formation. The first and simplest assumes a constant star formation rate for each galaxy from a starting redshift z_{in} to a final redshift z_{fin}. This constant level of star formation is determined separately for each galaxy, based on its mass and the available time. These models are referred to as *constant* models, and labelled as such in Figures 4–7. The boundaries correspond to star formation histories starting at an initial redshift, z_{in}, and finishing at a final redshift, z_{fin}, chosen to maximize or minimize the available time (i.e. bracket the range of reasonable star formation rates) and correspond to the minimum and maximum expected brightness, respectively. The constant models

assume no evolution in comoving volume density and a relatively quiescent star formation history. Galaxies which fit these models can also result from a bottom–up formation scenario, if we assume the galaxies were originally divided into N subsystems, each one forming stars in $\frac{1}{N}$ of the available time.

In the second class, each galaxy creates all its stars in a single burst over a fraction of the available time from z_{in} to z_{fin}. The observed luminosity function is thus shifted towards brighter galaxies which have lower density in their bright phase relative to galaxies which use the entire interval for star formation. We adopt a fractional interval of 0.2 and the same values of z_{in} and z_{fin} as in the constant models. These are labelled the *burst* models in Figures 4–7.

The third class of models assumes that most of the star formation takes place in small fragments or *subsystems* which later merge to form the final galaxy. We assume that star formation takes place at a constant rate over all of the available time and adopt five subsystems for this class. The assumption of a constant SFR in relatively small fragments results in a particularly low SFR in the subgalactic fragments, and thus these models are pessimistic for observers. Subdividing the galaxies into fragments shifts the resulting population toward more abundant but less luminous galaxies relative to the constant models. These are labelled the *hierarchical* models in Figures 4–7. The apparent brightness of L^* galaxies is indicated as a horizontal line on each model curve in all three figures.

It is likely that all three processes play some role in galaxy formation: merging is seen in the ultraluminous starburst galaxies, disks appear to grow continuously over Hubble timescales, and the high-redshift quasars imply rapid star formation at early times, perhaps in fragments much smaller than galaxies. There are few, if any, constraints on the free parameters in such a mixed model, but the general trend of particular mixes can be assessed by inspection of the plots, weighting the different classes for any hypothesis.

To follow the cosmic evolution of model expectations and survey results, there is a separate figure of comoving volume density vs. star formation rate for four redshift ranges. For each redshift range, the survey volume is restricted to that sampled by appropriate combinations of the five bright lines and the narrow filters' bandpasses, so the survey limits change somewhat among the four figures.

4.3.2. The redshift range $2 < z < 3.5$

This redshift range contains most of the known quasars in the fields and corresponds to the epoch of the maximum QSO density. At these redshifts, objects with unobscured star formation rates equal to $100\,\mathrm{M_\odot\,yr^{-1}}$ would be readily detected. The age of the universe was about $2.5\,\mathrm{Gyr}$ at $z = 2$ in the adopted cosmology. The maximum time available is long, and, therefore, the minimum luminosity is low, corresponding to a very long, quiescent phase of star formation. There is, however, no clear upper limit to the maximum luminosity, because the formation timescale

could be as short as desired, though this just represents a blurring of the distinction between the constant and burst models.

Figure 4 shows that the data sample enough volume to exclude the *constant* and *burst* models, although the limits only partially overlap the expectations for *hierarchical* models. Because the 90% detection probability limit line for this survey intersects the burst and constant models for galaxies fainter than L^*, statistical fluctuations in the (small) number of more massive galaxies present in any field will not change these conclusions. Young galaxies can be present in this redshift range only if they are small systems, have a low surface brightness, or are less efficient in emitting lines. Alternatively, the majority of galaxy formation could have occurred at higher redshifts.

The galaxies discovered by Steidel et al. (1996) have a lower density and/or a lower star formation rate (indicated by the heavy dashed line labelled S+96 in Figure 4) than any of the models. The velocity dispersions are similar to those seen in local spheroids and their density lower than the comoving density of L* galaxies found by Ellis et al. (1996) indicate that these are relatively massive systems. With their low apparent star formation rates (with typical values of about $8.5\,\mathrm{M}_\odot\,\mathrm{yr}^{-1}$), these galaxies would not be able to form all of the stars in an L* galaxy in the time available ($\sim 1\,\mathrm{Gyr}$) at a redshift of 3. Allowing the star formation to continue down to $z = 1.5$ and assuming a low-density cosmology would still be insufficient. Therefore, either a large fraction of the gas in these systems has yet to be converted into stars (if a constant SFR is assumed), the galaxy has already formed most of its stars (implying much higher star formation rates at earlier epochs), or sufficient dust exists in these objects to mask the true, higher star formation rates.

4.3.3.   The redshift range $3.5 < z < 5.5$

Figure 5 shows the redshift range corresponding to the appeerence of the QSO population. At these redshifts, galaxies with unobscured star formation rates of $200\,\mathrm{M}_\odot\,\mathrm{yr}^{-1}$ or more would have appeared in the survey, which is relatively high in comparison to known starburst galaxies at lower redshifts. The age of the universe at these redshifts is about $1\,\mathrm{Gyr}$. The models shown here use $z_{fin} = 3.5$, since later star formation should be detected preferentially by observations at the lower redshifts discussed in the previous section. The onset of star formation in these models begins at redshifts between 5.5 and 20.

At these higher redshifts, the data sample a sufficient volume to challenge the models: at least one galaxy should have been detected, if the *burst* models apply. There is also a significant overlap with the *constant* models, only those with the more quiescent star formation histories would escape detection. The *hierarchical* models are still fainter than the limits. As in the previous figure, the limit line intersects the *burst* and *constant* models above the L* value.

4.3.4. The redshift range $7 < z < 20$

Lyα (λ1215.7 Å) appears in the JHK' filters at redshifts between 8.3 and 18.7. There are several regions of good atmospheric transmission near 1 micron, of which both this survey and Parkes et al. (1994) make use, extending the observable redshift range down to $z \sim 7.2$. Figure 6 plots the restframe limits for this survey with Lyα in the J band, $7 < z < 10$. These redshifts may sample the parent population of galaxies which become quasars by $z > 4$. The universe at these redshifts was only $\sim 0.5\,$Gyr old. Even short bursts of star formation, lasting of order 10^8 yr, would span a $\Delta z > 1$, making surveys at these very high redshifts less sensitive to the exact timing of the onset of galaxy formation. Our deepest fields can detect an unobscured star formation rate of 220 M$_\odot$ yr^{-1}.

The K-band part of the survey includes a significant volume containing Lyα in the range $15.5 < z < 18.7$ (Figure 7). Our most sensitive data could detect star formation rates of 500 M$_\odot$ yr^{-1}, although the data do not go deep enough to significantly challenge the model predictions. They are meaningful if much of the star formation took place at these very high redshifts, in which case the star formation rates would necessarily be quite large.

5. Conclusions

Young galaxies with emission lines at infrared wavelengths are rare at the level of sensitivity and area coverage that can be reached with the current generation of detectors. This survey of 276 square arcminutes at a limiting sensitivity of approximately 3×10^{-16} ergs s^{-1} cm^{-2} in the J, H, and K$'$ bands revealed one emission-line object likely to be at $z = 2.43$.

The failure to detect many young galaxies makes it unlikely that most galaxies had star formation histories with continuous formation starting at any redshift and continuing to about $z \sim 2$. Hierarchical formation, in which galaxies were assembled from many pieces over a long interval are consistent with the results.

These conclusions stem from a comparison of the limits of the survey to calculations of expected line fluxes from various galaxy formation models. It is possible that physical conditions not included in the models could reduce the observable line strengths, and would weaken the conclusions derived from upper limits. Dust along the lines of sight to the galaxies could hide galaxies whose local line fluxes are above the detection limit (the effects of dust absorption are indicated in Figures 4–7). Young galaxies might be very extended, making the surface brightness too low to see in this survey, even though the overall line luminosities might be large.

Nevertheless, the availability of large-format infrared detectors makes it possible to conduct meaningful searches for high-redshift galaxies. The sensitivity reached by the present survey over the survey area is good enough to detect very young galaxies with a variety of possible star formation histories that can be considered "conventional." Increases in array sizes coupled with

wide-field optics make it attractive to continue the search for the first generation of stars at infrared wavelengths.

The combination of the sensitivity and area coverage of the present survey when compared with these conventional models underscores the importance of wide-field cameras to sample large volumes of the universe. Steidel et al. (1996) find 0.4 objects per square arcminute between $3.0 < z < 3.5$, or $\sim 4 \times 10^{-4}$ galaxies Mpc^{-3}. Several tens of such objects should be in the volume searched in the present work, although they would lie below the current detection limit. If the mass function for forming galaxies is reasonably approximated by the local one, as assumed in MB95 and the models used here, then the apparent number density of galaxies does not rise steeply with decreasing line flux. If these models are approximately correct, the higher sensitivity in the greatly restricted fields available on current or future large telescopes will be less effective in identifying a population of such objects than wide field searches.

This project is part of a continuing program at the Max-Planck-Institut für Astronomie to identify the formation of the first generation of galaxies, combining optical and infrared instrumentation to search a large volume of the parameter space available from the ground.

REFERENCES

Baron, E. & White, S. D. M. 1987, ApJ, 332, 585

Beckwith, S. V. W., Thompson, D. J., Mannucci, F., & Herbst, T. 1997, in preparation

Bessel, M. S., & Brett, J. M. 1988, PASP, 100, 1134

Börner, G., Mo, H. J., & Jing, Y. P. 1995, in *Galaxies in the Young Universe*, eds. H. Hippelein, K. Meisenheimer, & H.-J. Röser, (Springer, Heidelberg), 21

Boughn, S. P., Saulson, P. R., & Uson, J. M. 1986, ApJ, 301, 17

Bunker, A. J., Warren, S. J., Hewitt, P. C., & Clements, D. L. 1995, MNRAS, 273, 513

Casali, M. M. 1992, *JCMT UKIRT Newsletter*, 4, 33

Charlot, S. & Fall, S. M. 1993, ApJ, 415, 580

Coles, P. & Ellis, G. 1994, Nature, 370, 609

Collins, C. A., & Joseph, R. D. 1988, MNRAS, 235, 209

Cowie, L. L., Hu, E. M., & Songaila, A. 1995, Nature, 377, 603

Cowie, L. L., Songaila, A., & Hu, E. M. 1995, ApJ, submitted

De Propris, R., Pritchet, C. J., Hartwick, F. D. A., & Hickson, P. 1993, AJ, 105, 1243

Djorgovski, S., & Weir, N. 1990, ApJ, 351, 343

Dunlop, J., Peacock, J., Spinrad, H., Dey, A., Jimenez, R., Stern, D., & Windhorst, R. 1996, Nature, 381, 581

Efstathiou, G. 1995, in *Galaxies in the Young Universe*, eds. Hippelein, Meisenheimer, & Röser, (Springer, Heidelberg), 299

Efstathiou, G. 1996, in *HST and the High Redshift Universe*, 37th Herstmonceaux Conference, Cambridge, 1-5 July, 1996

Elias, J. H., Frogel, J. A., Matthews, K., & Neugebauer, G. 1982, AJ, 87, 1029

Ellis, R. S., Colless, M., Broadhurst, T., Heyl, J., Glazebrook, K. 1996, MNRAS, in press

Francis, P. J., Woodgate, B. E., Warren, S. J., Møller, P., Mazzolini, M., Bunker, A. J., Lowenthal, J. D., Williams, T. B., Minezaki, T., Kobayashi, Y., Yoshii, Y. 1996, ApJ, 457, 490

Freedman, W. L. et al. 1994, ApJ, 435, L31

Giavalisco, M., Steidel, C. C., & Macchetto, F. D. 1996, ApJ(?), in press

Haenelt, M. G., & Rees, M. J. 1993, MNRAS, 263, 168

Herbst, T. M., Beckwith, S. V. W., Birk, Ch., Hippler, S., McCaughrean, M. J., Mannucci, F., & Wolf, J. 1993, in *Infrared Detectors and Instrumentation*, SPIE Conference 1946, Fowler, A. M. (ed.), p. 605

Hewitt, A. & Burbidge, G. 1993, ApJS, 87, 451

Howell, S. B. 1989, PASP, 101, 616

Hu, E. M., & McMahon, R. G. 1996, Nature, 382, 231

Kennicutt, R. C. 1983, ApJ, 272, 54

Jarvis, J. F., & Tyson, J. A. 1981, AJ, 86, 476

Lu, L. Sargent, W. L. W., Womble, D. S., & Barlow, T. A. 1996, ApJ, 457, L1

Malkan, M., Teplitz, H., & McLean, I. 1995, ApJ, 448, L5

Malkan, M., Teplitz, H., & McLean, I. 1996, preprint

Mannucci, F., & Beckwith, S. V. W. 1995, ApJ, 442, 569

Mannucci, F., Beckwith, S. V. W., & McCaughrean, M. J. 1994, in *Infrared Astronomy with Arrays: the Next Generation*, I. S. McLean (ed), (Kluwer:Dordrecht), p. 503

McMahon, R. G., Omont, A., Bergeron, J., Kreysa, E., & Haslam, C. G. T. 1994, MNRAS, 267, L9

Meier, D. 1976, ApJ, 203, L103

Moorwood, A. et al. 1992, ESO Messenger, 69, 61

Mould, J. et al. 1995, ApJ, 449, 413

Pahre, M. A., & Djorgovski, S. G. 1995, ApJ, 449, L1

Parkes, I, Collins, C. A., & Joseph, R. D. 1994, MNRAS, 266, 983

Partridge, R. B. & Peebles, P. J. E. 1967, ApJ, 147, 868

Pritchet, C. J. 1994, PASP, 106, 1052

Pritchet, C. J., & Hartwick, F. D. A. 1987, ApJ, 320, 464

Pritchet, C. J., & Hartwick, F. D. A. 1990, ApJ, 355, L11

Schneider, D. P., Schmidt, M., & Gunn, J. E. 1991, AJ, 102, 837

Seaton, M. J. 1979, MNRAS, 187, 73P

Steidel, C. C., & Hamilton, D. 1992, AJ, 104, 941

Steidel, C. C., & Hamilton, D. 1993, AJ, 105, 2017

Steidel, C. C., Pettini, M., & Hamilton, D. 1995, AJ, 110, 2519

Steidel, C. C., Giavalisco, M., Pettini, M., Dickinson, M., & Adelberger, K. L. 1996, ApJ, in press

Terlevich, R. 1992, in *The Stellar Populations of Galaxies*, IAU Symp. 149, B. Barbuy & A. Renzini (eds.), (Dordrecht: Kluwer), p. 271.

Thompson, D., & Djorgovski, S. 1995, AJ, 110, 982

Thompson, D., & Djorgovski, S., & Beckwith, S. V. W. 1994, AJ, 107, 1

Thompson, D., Djorgovski, S., & Trauger, J 1995, AJ, 110, 963

Tinsley, B. M. 1977, ApJ, 211, 621

Tinsley, B. M. 1978, ApJ, 220, 816

Turner, E. L. 1991, AJ, 101, 5

Véron-Cetty, M.-P., & Véron, P. 1993, Catalog of Quasars and Active Nuclei, Sixth edition (ESO, Garching-bei-München)

Valdes, F 1989, in *First ESO/ST-ECF Data Analysis Workshop*, ESO Conf. proc. 31, P.J. Grosbol, F. Murtagh, & R.H. Warmels (eds.)

Wolfe, A. M., Turnshek, D. A., Smith, H. E., & Cohen, R. D. 1986, ApJS, 61, 249

TABLE 1. Observations

Field	R.A. (B1950) Dec.	z_{QSO}	Date	NB Filt. (μm)	Obs. Line	t_{nb} (min)	t_J (min)	t_H (min)	$t_{K'}$ (min)
Q 0040-279	00 40 12.2 −27 58 26	3.23	Aug 93[a]	2.121	[OIII]	54	15	15	21[b]
Q 0042-269	00 42 24.9 −26 56 33	3.358	Aug 93[a]	2.164	Hβ	67	14	14	14[b]
Q 0043-265	00 43 03.1 −26 33 33	3.44	Aug 93[a]	1.645	[OII]	83	14	14	14[b]
B2 0149+33	01 49 40.0 +33 35 46	2.431	Oct 93	2.260	Hα	91	26	$\cdots$	26
			Dec 94	2.248	Hα	106	26	26	39
Q0259+0112	02 59 02.8 +01 12 56	2.316	Dec 94	2.166	Hα	104	$\cdots$	$\cdots$	26
US 3342	02 52 40.2 +01 36 26	2.457	Oct 93	2.260	Hα	95	26	$\cdots$	26
PKS 0504+03	05 04 59.3 +03 03 59	2.463	Oct 93	2.260	Hα	93	$\cdots$	$\cdots$	52
			Dec 94	1.282	[OII][d]	104	26	26	26
OH 471	06 42 53.0 +44 54 31	3.408	Oct 93	1.644	[OII]	81	$\cdots$	12	$\cdots$
B3 0806+426	08 06 37.9 +42 36 56	1.184	Dec 94	1.094	[OIII]	71	13	13	13
B2 0812+33A	08 12 24.0 +33 14 42	2.420	Dec 94	2.248	Hα	208	$\cdots$	$\cdots$	26
			Dec 94	1.282	[OII]	53	26	$\cdots$	$\cdots$
MG 0827+1052	08 24 22.4 +11 02 19	2.295	Dec 94	2.166	Hα	104	$\cdots$	$\cdots$	52
B2 0902+34	09 02 24.8 +34 19 58	3.395	Feb 93	1.644	[OII]	79	$\cdots$	29	32
Q 1159+123	11 59 14.2 +12 23 12	3.502	May 93	2.248	[OIII]	87	$\cdots$	$\cdots$	20
			Jun 94	2.248	[OIII]	80	$\cdots$	$\cdots$	39
			Dec 94	2.248	[OIII]	199	17	$\cdots$	35
1332.8+2611	13 32 50.6 +26 11 55	2.503	May 93	2.295	Hα	92	$\cdots$	$\cdots$	52[e]
			Jun 94	2.295	Hα	69	$\cdots$	$\cdots$	39
Q 1336+2534	13 36 40.9 +25 34 19	2.242	Dec 94	2.122	Hα	52	$\cdots$	$\cdots$	26
1440-232	14 40 08.0 −23 16 32	2.221	Aug 93[a]	2.121	Hα	106	14	14	40[b]
TEX 1559+140	15 59 35.2 +14 05 29	2.237	Feb 93	2.122	Hα	36	$\cdots$	$\cdots$	30
PC 1619+4631	16 19 51.3 +46 31 25	3.471	May 93	2.248	[OIII]	130	$\cdots$	$\cdots$	65
Blank 1[f]	16 33 06.5 +33 31 18	$\cdots$	Jun 94	2.248	$\cdots$	62	$\cdots$	$\cdots$	39
Blank 2[f]	16 33 06.5 +33 31 18	$\cdots$	Jun 94	2.295	$\cdots$	61	$\cdots$	$\cdots$	$\cdots$
Blank 3	16 56 25.0 +33 58 00	$\cdots$	Jun 94	2.295	$\cdots$	52	101	105	$\cdots$
Blank 4	17 38 00.0 +35 00 00	$\cdots$	May 93	2.166	$\cdots$	134	$\cdots$	$\cdots$	38
4C 47.48	18 16 58.7 +47 35 26	2.230	May 93	2.122	Hα	125	$\cdots$	$\cdots$	33
2113.3+0575	21 13 18.1 +05 44 45	2.463	Dec 94	2.122	Hα	97	$\cdots$	$\cdots$	26[c]
PKS 2126-15	21 26 26.7 −15 51 51	3.266	Aug 93[a]	2.136	[OIII]	94	$\cdots$	14	14[b]
PKS 2136+141	21 36 37.4 +14 10 01	2.427	Oct 93	1.282	[OII]	90	25	$\cdots$	26
2359+0653	23 59 06.8 +06 53 13	3.238	Oct 93	2.122	[OIII]	102	13	$\cdots$	26

[a]Data taken at the La Silla ESO-MPI 2.2m telescope.

[b]Data taken through a Ks filter.

[c]Data taken through a standard K filter.

[d]The target line lies just outside the filter bandpass.

[e]Includes 26 min obtained in Dec 1994.

[f]A quasar, WEE 148, is present in the field, though its emission lines lie outside the narrowband filters.

Table 2. Results

| Field	NB filter (μm)	PSF FHWM (arcsec)	Area (sq. arcmin)	3σ Flux Limit 10^{-16} erg sec^{-1} cm^{-2}
Q 0040-279	2.121	1.2	5.2	3.7
Q 0042-269	2.164	1.8	4.9	5.9
Q 0043-265	1.645	1.8	4.3	9.1
B2 0149+33	2.260	1.7	12.5	2.8
B2 0149+33	2.248	1.8	11.6	1.9
Q0259+0112	2.166	2.8	10.3	4.2
US 3342	2.260	1.3	12.4	2.2
PKS 0504+03	2.260	2.2	12.3	3.7
PKS 0504+03	1.282	2.1	11.7	4.0
OH 471	1.644	1.6	12.1	1.8
B3 0806+426	1.094	1.6	9.8	3.2
B2 0812+33A	2.248	2.8	11.3	4.9
B2 0812+33A	1.282	2.0	10.6	5.1
MG 0827+1052	2.166	2.2	10.8	3.1
B2 0902+34	1.644	1.8	10.8	2.1
Q 1159+123	2.248	1.8	9.5	1.6
1332.8+2611	2.295	2.0	8.5	2.9
1336.7+2534	2.122	2.1	10.0	3.0
1440-232	2.121	1.5	6.1	4.9
TEX 1559+140	2.166	1.8	11.3	8.1
PC 1619+4631	2.248	2.6	11.2	4.0
Blank 1	2.248	1.4	13.3	3.3
Blank 2	2.295	1.4	13.3	3.4
Blank 3	2.295	1.1	12.1	3.7
Blank 4	2.166	1.5	9.1	1.4
4C 47.48	2.166	1.6	12.3	1.4
2113.3+0575	2.260	1.4	12.7	2.9
PKS 2126-15	2.136	1.2	4.4	5.1
PKS 2136+141	1.282	2.2	12.0	4.6
2359+0653	2.122	1.8	14.1	1.6
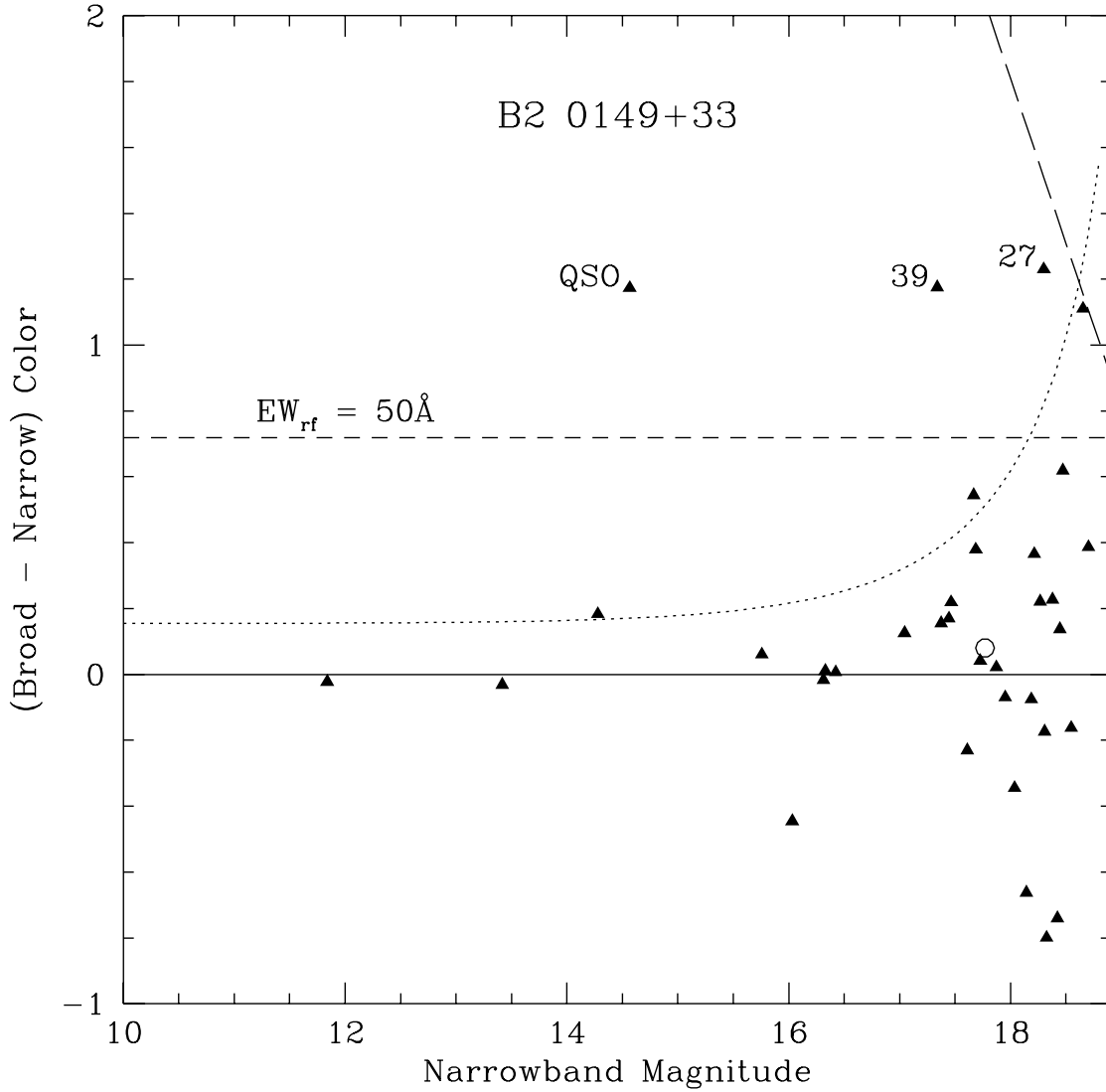
Fig. 1.— Color-magnitude diagram for the B2 0149+33 field. The curved line indicates 3σ emission line flux, while the horizontal dashed line is set to an emission line equivalent width of 50Å in the restframe of the quasar. Objects to the left of the diagonal long-dashed line are well-detected in both images. The quasar and objects #39 (the emission line candidate) and #27 (see text) are labelled, while the galaxy next to the quasar is marked with an open circle.

Fig. 2.— Images of the B2 0149+33 field through the broad (left) and narrowband (right) filters. The quasar (tick mark) and the emission line object #39 (arrowed) are indicated. The images are oriented with north up and east to the left, and are scaled so that continuum objects appear the same in both images. Emission-line objects, such as the quasar and object #39, appear brighter in the narrowband image.
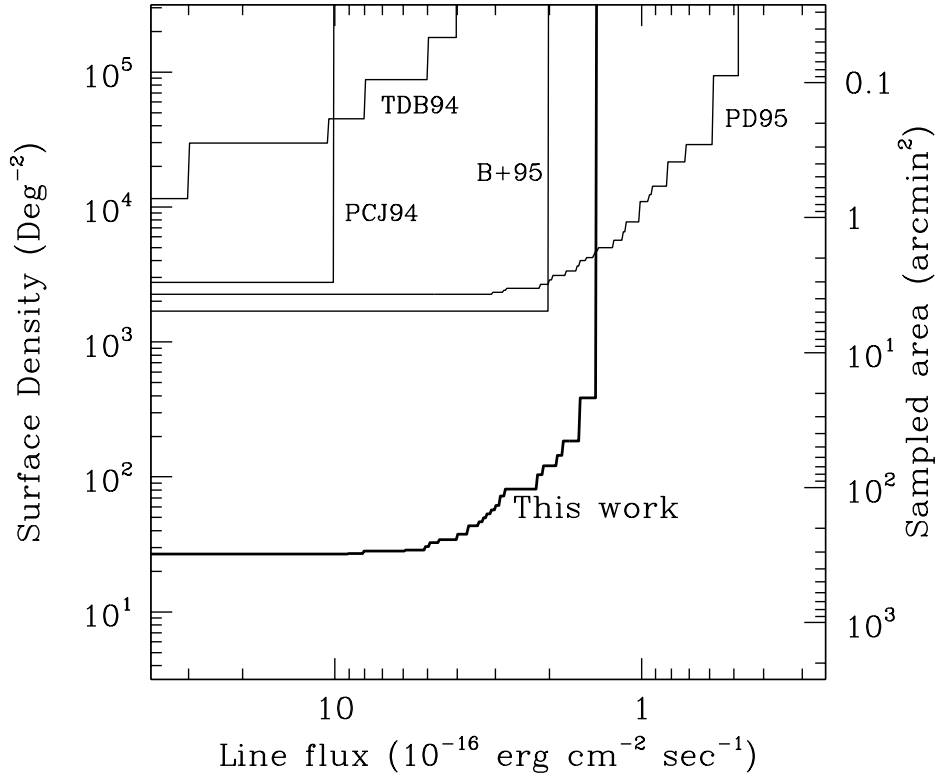
Fig. 3.— Comparison between the various published NIR emission-line surveys. The vertical scale on the right is the sampled area, the one on the left is the minumum detectable surface density at 90% confidence. The thick line is the limit from this work, while the thin lines are the limits from other published work (PD95: Pahre and Djorgovski, 1995; TDB94: Thompson, Djorgovski and Beckwith, 1994; B+95: Bunker et al, 1995; PCJ94: Parkes, Collins and Joseph, 1994).
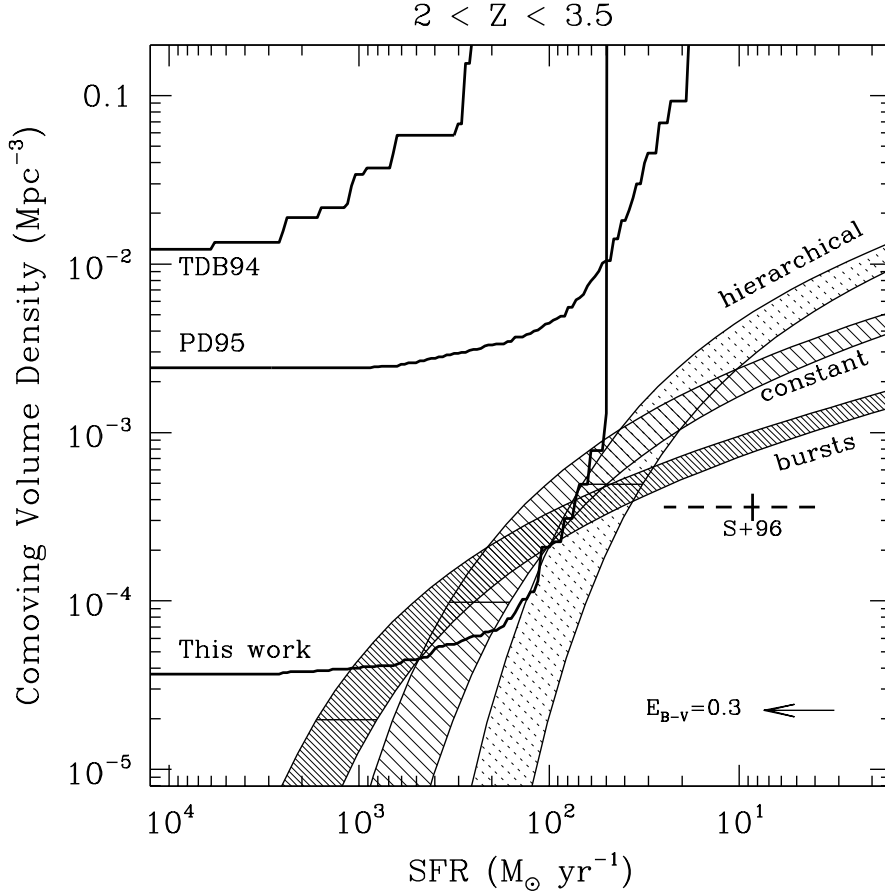
Fig. 4.— Restframe limits in the redshift range $2.0 < z < 3.5$. In our data, this redshift range is sampled primarily by Hα and [OIII] in the K band. The three classes of models, descibed in the text, are labeled as *constant, burst* and *hierarchical*. For each class of model, we used $z_{fin} = 2$ and $3.5 < z_{in} < 20$. At any given SFR, the model lines indicate the expected comoving density of objects with at least this level of star formation. The horizontal lines across each model region show the position of the L* galaxies. The dashed line marks the comoving density $(3.6 \times 10^{-4}$ Mpc$^{-3})$ and range of SFR (4-25 M$_\odot$ yr^{-1}) for the population of star-forming galaxies detected by Steidel et al. (1996) at $3.0 < z < 3.5$, while the mark at 8.5 M$_\odot$ yr^{-1} indicates a "typical" SFR as reported by the authors. The three thick lines are the upper limits to the PG volume density from three surveys (this work; TDB94: Thompson, Djorgovski and Beckwith, 1994; PD95: Pahre and Djorgovski, 1995), where the regions to the upper right of these curves are excluded by the surveys. If sufficient dust were present in the galaxies to cause $\sim 1^m$ extinction at visual wavelengths, the limit lines should be moved to the left by the amount indicated by the arrow.
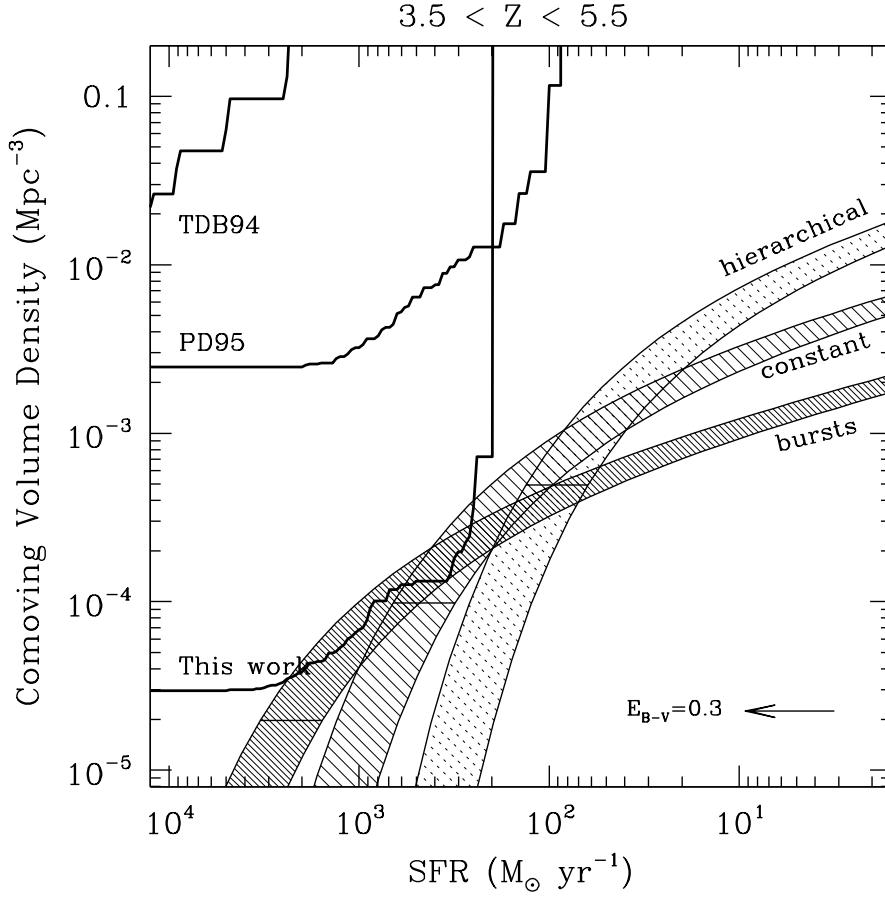
Fig. 5.— Restframe limits in the redshift range $3.5 < z < 5.5$. This redshift range is sampled by [O II] in the H and K bands, and by Hβ and [O III] in the K band. The models are as in Figure 4, with $z_{fin} = 3.5$ and $5.5 < z_{in} < 20$. The effects of dust on these bluer emission lines is again indicated by the arrow.
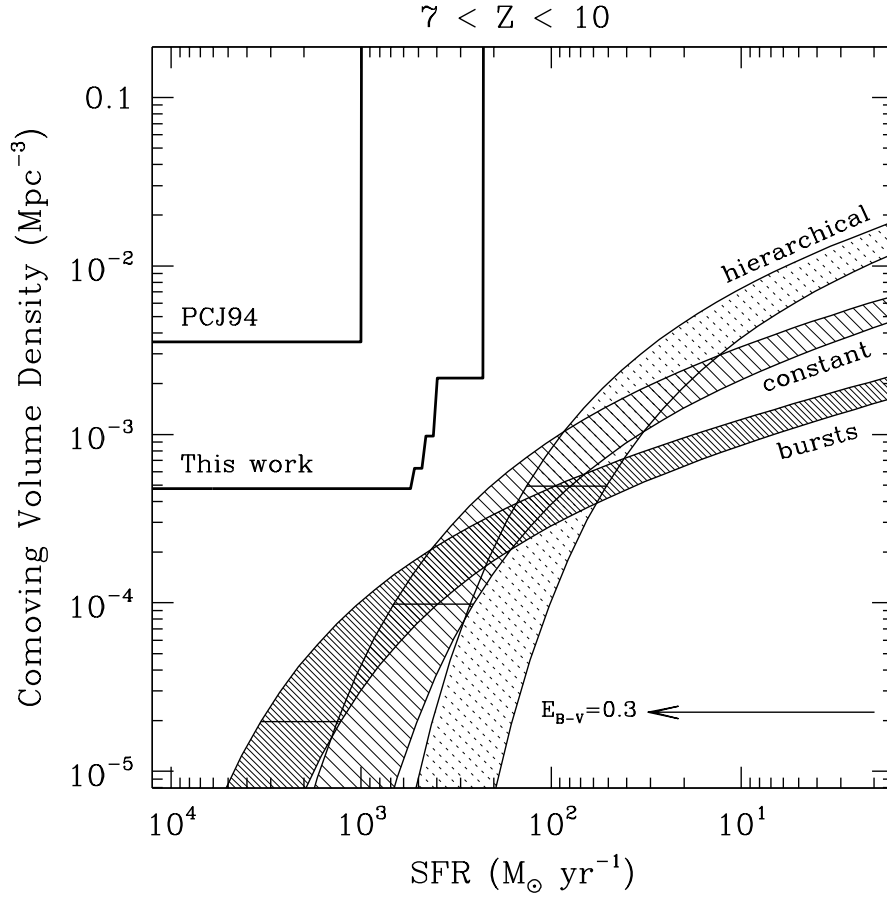
Fig. 6.— Restframe limits for Lyα in the J band ($7.0 < z < 10$). The models are the same as in Figure 4, with $3 < z_{fin} < 6$ and $z_{in} = 20$. For the Lyα line, z_{fin} is varied rather than z_{in}, and z_{fin} is allowed to extend to lower redshifts, otherwise the time available at these high redshifts would be unreasonably short. Dust extinction corresponding to $A_V \sim 1^m$, *neglecting resonant scattering*, is indicated by the arrow.
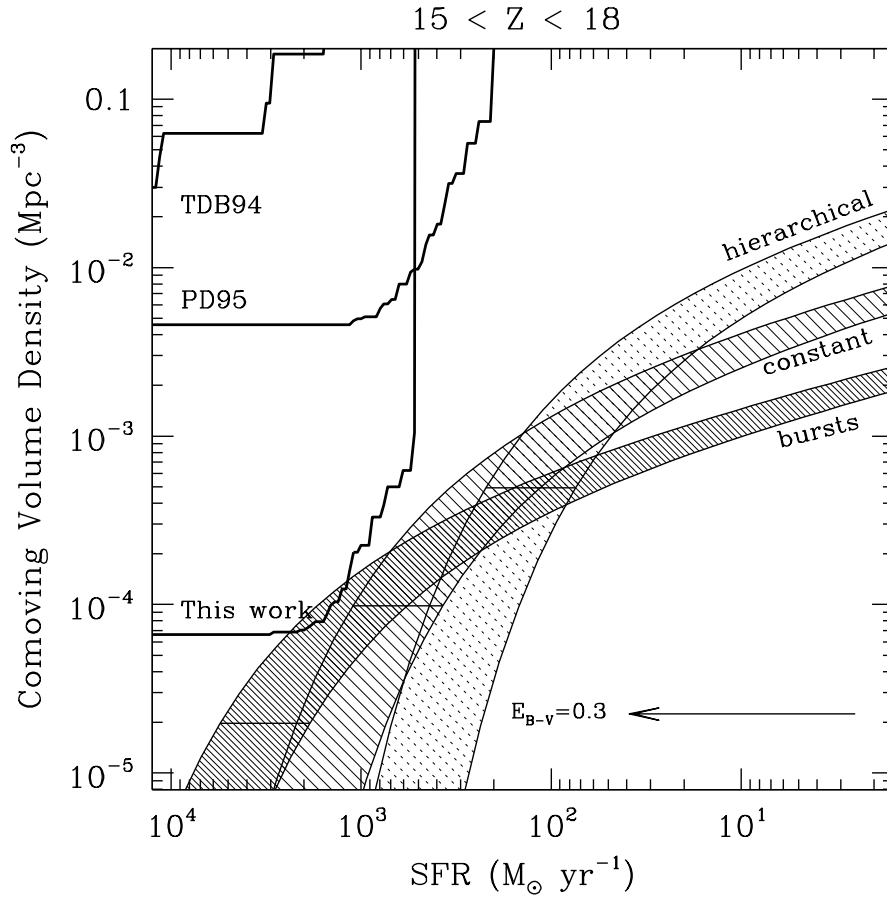
Fig. 7.— Restframe limits for Lyα in the K band ($15 < z < 18$). The models are the same as in Figure 6, with $4 < z_{fin} < 8$ and $z_{in} = 20$. Extinction by dust, as in the previous figure, is indicated by the arrow.